






Classification of Yu-Shiba-Rusinov states of magnetic impurities on superconducting surfaces: A fully relativistic first-principles study

András Lászlóffy ¹, Bendegúz Nyári ^{2,3}, László Szunyogh ^{2,3}, Kyungwha Park ⁴, and Balázs Ujfalussy ¹

¹*Wigner Research Centre for Physics, Institute for Solid State Physics and Optics, H-1525 Budapest, Hungary*

²*Department of Theoretical Physics, Institute of Physics, Budapest University of Technology and Economics, Műegyetem rakpart 3, H-1111 Budapest, Hungary*

³*ELKH-BME Condensed Matter Research Group, Budapest University of Technology and Economics, Műegyetem rakpart 3, H-1111 Budapest, Hungary*

⁴*Department of Physics, Virginia Tech, Blacksburg, Virginia 24061, USA*



(Received 6 April 2023; accepted 31 May 2023; published 23 June 2023)

Magnetic adatoms at surfaces of superconductors may induce localized bound states within the superconducting energy gap referred to as Yu-Shiba-Rusinov (YSR) states. We solve the Kohn-Sham-Dirac Bogoliubov–de Gennes equations within the fully relativistic multiple scattering Green’s function method to study the nature of the YSR states for $3d$ magnetic impurities (Cr, Mn, Fe, and Co) placed on a pristine Nb(110) surface, as well as capped by a monolayer of Bi, Re, or Ir. First, we perform self-consistent relativistic calculations in the normal state and determine the direction of the easy axis and the magnetic anisotropy energy. Then we study the relation between the electronic structure in the normal state and the YSR states. We show that the YSR states can be categorized according to the energy-resolved singlet and triplet order parameters as normal, superconducting singlet, or induced triplet states. Finally, we demonstrate that the rotation of the adatom magnetic moment shifts the energy of the YSR states as a consequence of the spin orbit coupling. During this rotation, some branches of the YSR states might cross the Fermi energy, implying that at certain paths in the configuration space a peak can be found at zero energy.

DOI: [10.1103/PhysRevB.107.224515](https://doi.org/10.1103/PhysRevB.107.224515)

I. INTRODUCTION

It is well known that a strong local magnetic field breaks the Cooper pairs in conventional superconductors. Depositing a single magnetic atom onto the surface of a superconductor can induce in-gap bound states, which are known as Yu-Shiba-Rusinov (YSR) states [1–3]. It has been theoretically proposed that the arrangement of several magnetic impurities induces hybridization of the YSR states and can lead to the formation of Majorana zero modes (MZMs) [4–15]. The experimental progress hints at the existence of such MZMs; however, it is not easy to uniquely identify them [16–19]. This is so even if scanning tunneling microscopy technology using superconducting tips has sufficient resolution to resolve multiple YSR states at subgap energies. Furthermore, experiments nowadays are able to show even the hybridization of YSR states in adatom dimers [15–18,20].

Investigating the material-specific fundamentals of the YSR states [21–25] is not only an important step towards understanding local excitations in superconductors and the interpretation of experiments but also a first step towards designing new, artificial Majorana systems as well. Such calculations have the additional benefit of exploring quantities which are difficult or impossible to achieve with measurements, like the magnetic anisotropy energy or the superconducting order parameter, allowing a complex characterization of the YSR states. In the current paper we present first-principles-based calculations for various magnetic

impurities on the surface of Nb(110) and Nb(110) covered by various single-atom-thick overlayers of heavy elements. The main idea behind depositing different overlayers on the surface is to tune the spin-orbit coupling (SOC) in the system while hosting the same, rather large superconducting gap of Nb. Such systems can often be realized in an experimental situation depending on growth conditions [26,27].

In what follows in Sec. II we summarize the computational details of solving the Dirac–Bogoliubov–de Gennes equations within the multiple scattering theory (MST). In Sec. III A we present the results for single $3d$ magnetic impurities (Cr, Mn, Fe, and Co) on the Nb(110) surface and show some relationships between the obtained YSR states and the normal density of states. In Sec. III B we turn to the study of magnetic impurities on Bi, Re, and Ir overlayers on Nb(110). Adding an overlayer to Nb(110) has two effects: it changes the strength of the SOC and also changes the electronic states of the impurity in the normal state, both of them remarkably influencing the YSR states induced by the impurity. We also analyze the effects of SOC through the appearance of a spin triplet superconducting order parameter and by rotating the direction of the magnetic moment. Finally, in Sec. IV we draw the conclusions of our work.

II. COMPUTATIONAL DETAILS

The computational methods used in this work were already published in Ref. [24], and here we shall mainly

focus on describing the geometry of the considered systems and on the parametrization of the screened Korringa-Kohn-Rostoker calculations. To briefly summarize the method, first, we achieve charge self-consistency for the surface impurity system in the normal state using standard density functional theory via the embedded Green's function technique within MST [28]. Then we continue by solving the fully relativistic Dirac–Bogoliubov–de Gennes (DBdG) equations (1), yet again within MST, using the self-consistent potentials obtained during the first step of the calculation:

$$\left[\varepsilon - \begin{pmatrix} H_D & \Delta_{\text{eff}} \\ \Delta_{\text{eff}}^\dagger & -H_D^* \end{pmatrix} \right] \begin{pmatrix} \Psi_u(\varepsilon) \\ \Psi_v(\varepsilon) \end{pmatrix} = 0, \quad (1)$$

where ε is the energy relative to the Fermi energy E_F , $\Psi_u(\varepsilon)$ and $\Psi_v(\varepsilon)$ are the four-component electron- and holelike parts of the wave function, respectively, Δ_{eff} is the effective pair interaction, and H_D is the Kohn-Sham-Dirac Hamiltonian; see, e.g., Ref. [24] and the Appendix for more details. Local densities of states and order parameters in the superconducting state are calculated from the MST Green's function of the DBdG Hamiltonian (see Ref. [29]). It is worth pointing out that our approach has the advantage of avoiding a supercell approach at any step of the calculation.

In what follows, we present results for single magnetic adatoms on bare Nb and metallic overlayers on a Nb(110) surface. Beyond the bare Nb(110) surface, we also consider a single-atom-thick overlayer of Bi, Re, or Ir on top of the semi-infinite Nb surface. The magnetic adatom, either Co, Fe, Mn, or Cr, is embedded in the first vacuum layer above the surface/overlayer. For simplicity (and comparability), we assumed ideal epitaxial positions of all atoms. In the spirit of the embedded cluster method, beyond the adatom, the embedded cluster also contained the atoms of the host surface within a radius of $\sqrt{3}a_{\text{Nb}}$ (with $a_{\text{Nb}} = 330.04$ pm being the bulk lattice constant): 7 Nb atoms from the layer just below the surface; 14 Nb, Bi, Re, or Ir atoms from the surface layer; and, additionally, 30 lattice sites from the first two layers above the surface representing the vacuum. Altogether, the effective potentials and exchange fields on 52 sites were allowed to relax due to the presence of the impurity in the self-consistent cycles. We also performed calculations with different cluster sizes and concluded that the clusters presented are sufficiently large to determine the energy of the YSR states.

First, we performed self-consistent field (SCF) calculations with magnetization pointing along the $z = [110]$ axis. In order to obtain the ground state orientation of the magnetization for each adatom system, the magnetocrystalline anisotropy energy (MAE) was determined for each cluster from a tensorial spin model based on the spin-cluster expansion technique [30,31], which in turn indicated that the easy direction can be any of $x = [\bar{1}10]$, $y = [001]$, or z , depending on the actual system. Next, we repeated the SCF calculations with the direction of the magnetic moment pointing along the easy direction (if it was not the z direction) to obtain the ground state potentials. The values for the magnetic moment, the obtained easy direction, and the calculated MAE are collected in Table I.

When performing calculations in the superconducting state, we assumed that the opening of the narrow

TABLE I. Calculated spin magnetic moments M_s (in units of μ_B), the easy direction \vec{s}_e , and the anisotropy energies $E_x - E_z$ and $E_y - E_z$ (meV) for all the magnetic adatom systems considered.

System	M_s	\vec{s}_e	$E_x - E_z$	$E_y - E_z$
Cr/Nb(110)	4.25	y	-0.20	-0.25
Mn/Nb(110)	4.26	z	0.17	0.36
Fe/Nb(110)	3.12	z	1.50	1.73
Co/Nb(110)	1.75	z	2.86	3.45
Cr/Bi/Nb(110)	4.49	y	-0.07	-0.66
Mn/Bi/Nb(110)	4.31	z	0.20	0.30
Fe/Bi/Nb(110)	3.14	z	2.74	2.09
Co/Bi/Nb(110)	1.84	x	-0.91	0.04
Cr/Re/Nb(110)	4.22	z	1.76	5.41
Mn/Re/Nb(110)	4.42	z	2.06	1.85
Fe/Re/Nb(110)	3.29	y	0.21	-4.56
Co/Re/Nb(110)	2.00	y	-5.25	-9.12
Cr/Ir/Nb(110)	4.36	y	0.57	-3.61
Mn/Ir/Nb(110)	4.61	y	-0.93	-1.22
Fe/Ir/Nb(110)	3.50	x	-0.67	5.82
Co/Ir/Nb(110)	2.22	z	3.98	11.79

superconducting gap has only a marginal effect on the charge and magnetization densities; therefore, we did not attempt to achieve charge self-consistency in the superconducting state. The effective pairing potential Δ_{eff} was regarded as a constant fitted to the experimental value of the superconducting gap of Nb, $\Delta_{\text{Nb}} = 1.51$ meV [20]. On the magnetic adatom and in the vacuum we assumed $\Delta_{\text{eff}} = 0$.

III. RESULTS

A. Adatoms on Nb(110) surface

From the normal state SCF calculations we obtained rather large spin moments of $4.25\mu_B$ and $4.26\mu_B$ for the Cr and Mn adatoms on the Nb(110) surface, respectively (see the top block in Table I). This can be explained by the occupation of the majority (spin-up) and minority (spin-down) channels that can be inferred from the spin-resolved local densities of states (LDOSs) depicted in Fig. 1. In the case of the Cr adatom, 85%

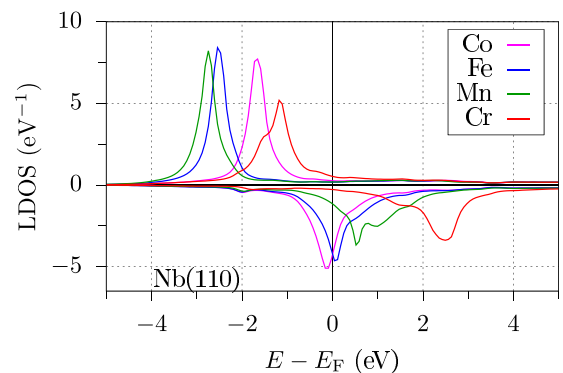


FIG. 1. LDOS of magnetic adatoms on a Nb(110) surface in the normal state. Positive values: LDOS in the majority spin channel; negative values: LDOS in the minority spin channel multiplied by -1 . The Fermi energy is denoted by a vertical black line at $E = 0$.

of the majority spin channel is filled, while the minority spin channel is empty (its occupation is less than 5%). In addition, the LDOS at the Fermi level is small because the Fermi energy lies between the well-separated spin-down and spin-up peaks. In the case of the Mn adatom, the majority and minority spin channels are occupied to an extent of 95% and 15%, respectively. Relative to the Cr adatom, the larger occupation of the minority channel results in a larger LDOS at the Fermi energy. For the Fe and Co adatoms, about 93% of the majority channel is filled, and the minority channel becomes increasingly occupied with an increasing atomic number, i.e., with an increasing number of electrons for these atoms. Compared to those of Cr and Mn, the spin magnetic moment decreases to $3.12\mu_B$ for the Fe adatom and to $1.75\mu_B$ for Co. Concomitant with the downwards shift of the minority band, the value of the normal state LDOS is significantly larger at the Fermi energy for Fe and Co. Note that the splitting of the majority and minority bands, defined as the energy difference of the maxima of the corresponding LDOSs, is a monotonically increasing function of the spin magnetic moment: the exchange splittings are around 3.5 eV for the Cr and Mn adatoms and 2.7 eV for the Fe adatom, and it is significantly reduced in the case of Co, where it is around 1.7 eV.

As mentioned in Sec. II, the SCF calculations were performed for the ground state orientation of the magnetic moment, which is parallel to the z axis for Mn, Fe, and Co atoms, but it is along the y axis for the Cr adatom (see Table I). A small MAE is expected for the Cr and Mn adatoms [32], for which the majority band is fully occupied and the occupation at the Fermi energy is low. For the Fe and Co adatoms the minority band is partly occupied, and its peak lies close to the Fermi energy, which leads to a large MAE, even reaching 3.45 meV for the Co adatom. Note that the Mn, Fe, and Co adatoms share not only the easy axis (z) but also the medium (x) and hard (y) directions because in these cases $E_y - E_z > E_x - E_z \Rightarrow E_y > E_x$.

In Fig. 2 the LDOS of the magnetic adatoms in the superconducting state is shown. We found that the superconducting LDOS scales with the normal state LDOS at the Fermi energy, so in order to be able to show them on the same plot we present the LDOS in the superconducting state divided by the normal state LDOS at E_F . Also, since our calculations are fully relativistic, with SOC implicitly included, the LDOS cannot uniquely be projected to d orbitals and spin components. However, if the effect of SOC is weak and, consequently, the energy spectrum only slightly changes with respect to the nonrelativistic case, such a projection can be illustrative even for the relativistic case (see, e.g., for the Mn adatom [24,25,33]).

For all the adatoms one can see the appearance of YSR states in the superconducting gap. Since the investigated adatoms are all transition metal elements, we expect a maximum of five pairs of peaks related to the d orbitals in the superconducting gap. Several works showed that scaling the magnetic moment shifts the position of the YSR states [2,3,20,24,34]. Inferring from Figs. 1 and 2 we can see a straightforward relationship between the position of the YSR states and the spin polarization of the LDOS at the Fermi energy in the normal state. For the low spin polarization of the LDOS in the case of the Cr adatom the YSR states appear

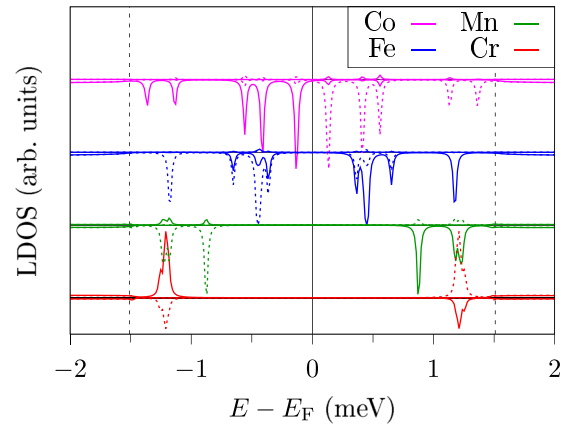


FIG. 2. Calculated LDOS in the superconducting gap of the adatoms on the bare Nb(110) surface. For better visibility, the baseline is shifted for the different adatoms. Solid and dashed lines label the electron and hole parts of the LDOS, while above and below the baseline the spin-up and spin-down components can be seen, respectively. The Fermi energy and the superconducting gap are denoted by solid (at $E - E_F = 0$) and dashed (at $E - E_F = \pm\Delta_{\text{Nb}}$) vertical lines, respectively.

near the edges of the gap. With increasing spin polarization the positions of the YSR peaks get shifted towards the center of the gap, and also new YSR states appear in the spectrum. Investigating the electron and hole parts of the YSR peaks, we can conclude that for the largest spin polarization in the case of the Fe and Co adatoms some or even all of the YSR peaks appear on the opposite side of the Fermi level. Such crossings of the Fermi level in the energetic position of the YSR states were clearly demonstrated in Ref. [20] (see Supplemental Material, Fig. 11) as a function of the spin parameter of a multiorbital tight-binding model.

In the case of the Cr adatom, the electron spin-up (electron up for short) and hole spin-down (hole down) components are mixed at the peak below E_F , while due to particle-hole symmetry the electron down and hole up components are mixed at the peak above E_F . This is an indication of a superconducting state; consequently, we may associate this kind of mixing with Cooper pair scattering.

The YSR states of the Co adatom display a very different behavior. There are five pairs of YSR peaks well separated in energy. Below the Fermi energy the peaks have only the electron down component, while above E_F they have only the hole down component, with unremarkable electron-hole mixing. Such behavior is a signature of the solution of the Bogoliubov–de Gennes equations with zero effective pair interaction ($\Delta = 0$). Consequently, these states behave like excitations with large spin polarization in the normal state which completely breaks the Cooper pairs.

The LDOS for Mn and Fe adatoms shows features qualitatively similar to Co: the YSR states have large spin-down electron or tiny spin-up electron components. It should be mentioned that for the Fe adatom only four YSR states can be seen; however, a more detailed calculation with higher resolution revealed that one of the peaks is actually composed of two peaks that are very close to each other.

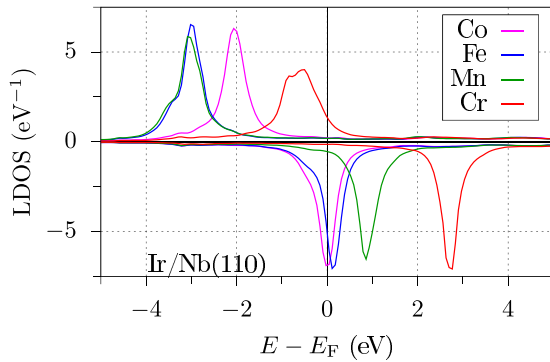


FIG. 3. Normal LDOS of magnetic adatoms on the Ir overlayer on a Nb(110) surface in units of $1/\text{eV}$. Positive values: LDOS of the majority spin channel; negative values: LDOS of the minority spin channel multiplied by -1 . The Fermi energy is denoted by a vertical black line at $E = 0$.

B. Adatoms on metallic overlayers with large SOC on Nb(110) surface

Although in relativistic multiple scattering theory it is possible to scale the SOC [35], in order to provide a realistic scenario for experiments, here we elected to do it by adding a single layer of Bi, Re, or Ir on top of the semi-infinite Nb(110). The corresponding figures with SOC scaled to zero can be found in the Supplemental Material [36]. According to our calculations, the proximity-induced superconducting gap is around the same size as in Nb bulk if only single atomic layer coverage is considered in these systems (for larger coverages see Refs. [27,37]). We performed SCF calculations for magnetic adatoms (Cr, Mn, Fe, or Co) on a single Bi, Re, or Ir overlayer on a Nb(110) surface in the normal state and present the results in Table I. The magnetic moment of the Cr adatom (being between $4.22\mu_B$ and $4.49\mu_B$) and Mn ($4.26\mu_B$ – $4.61\mu_B$) changes by only 8% if the overlayer is changed; however, it changes in a relative range of 12% for the Fe adatom ($3.12\mu_B$ – $3.50\mu_B$) and 25% for the Co adatom ($1.75\mu_B$ – $2.22\mu_B$). The robustness of the Cr and Mn moments can be explained by the almost filled majority and nearly empty minority spin channels.

The general features of the impurity LDOS in the normal state with the different overlayers differ only slightly from their bare Nb counterparts. As an example the case of an Ir overlayer is shown in Fig. 3. Remarkably, the dispersion of the majority band of the adatoms is enhanced, while that of the minority band is reduced relative to the case of a bare Nb surface. This is the consequence of the almost fully occupied Ir d band, which suppresses the hybridization in the minority spin channel.

Contrary to the LDOS, the magnetic anisotropy energy and the easy direction of the magnetization strongly depend on the overlayer (see Table I). In the case of the Bi overlayer, we get the same sign for the anisotropy energies as in the uncovered case, leading to the same easy directions, except for the Co adatom, for which the magnitude of the energies is significantly reduced and also the sign of $E_x - E_z$ is reversed, which rotates the easy direction to x . The magnetic anisotropies are definitely different for the cases of the Re and

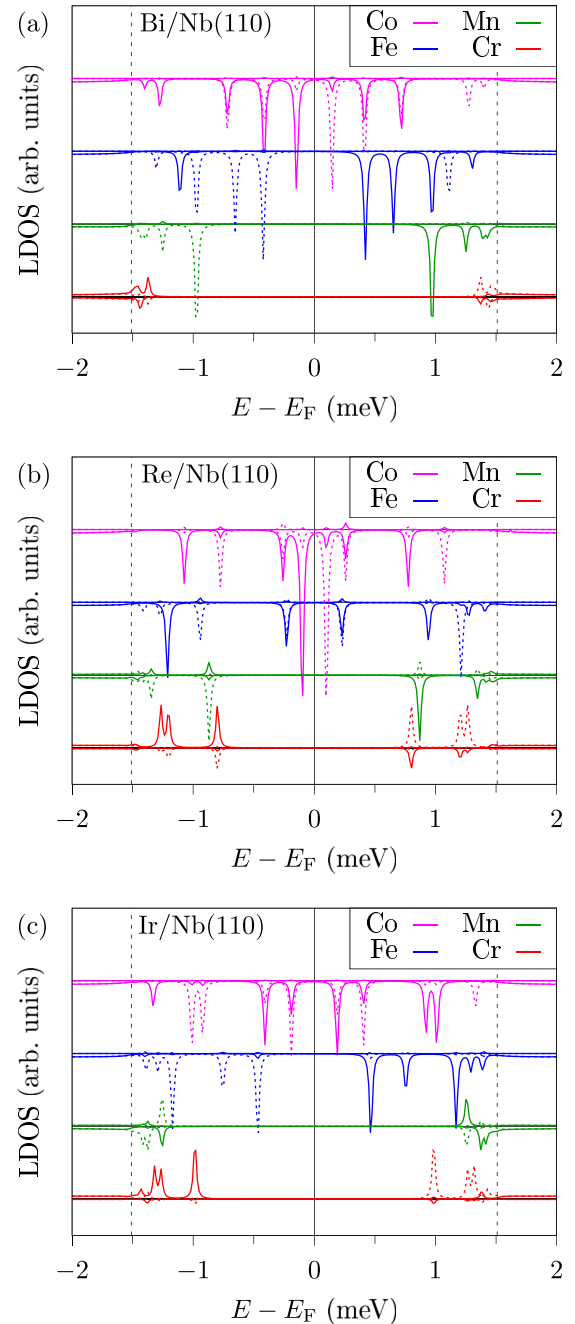


FIG. 4. Calculated LDOS in the superconducting gap of the adatoms on the overlayer systems. Solid and dashed lines label the electron and hole parts of the LDOS, while above and below the baseline the spin-up and spin-down components can be seen, respectively. (a) Bi overlayer, (b) Re overlayer, and (c) Ir overlayer.

Ir overlayers. Even though the SOC is expected to be larger with Bi, the hybridization with the substrate may be weaker. The SOC is still strong in Re and Ir; a larger hybridization of the adatom with the Re or Ir overlayer leads to a change in the easy axis with increasing MAE. This can be seen most illustratively for the Fe adatom, which has z , y , and x easy directions in the case of the Bi, Re, and Ir overlayers, respectively. The superconducting LDOSs of the adatoms on various overlayers are shown in Fig. 4. In the case of a Bi overlayer [Fig. 4(a)]

one can see five pairs of peaks with a clear separation in the cases of the Co and Fe atoms. There are four pairs of peaks in the case the Mn atom, where the two peaks closest to the edges of the gap strongly overlap with each other. For the Cr adatom we obtain two peaks with energy being very close to the edge of the gap. The Re overlayer is more interesting in the sense that Re is also a superconducting material, albeit with a smaller gap and lower superconducting critical temperature. In this particular case, however, we found that, independent of whether we use a pairing potential $\Delta = 0.28$ meV (the same as the superconducting gap measured in Ref. [38]) or $\Delta = 0$ in the Re layer, the induced superconducting gap in the calculated LDOS determined by Nb bulk is not affected. For the Re overlayer we also find that the lowest energy YSR state in the superconducting gap typically lies closer to the Fermi energy than previously seen (except for the Mn atom); for example, there is a YSR state at $E = 80 \mu\text{eV}$ in the case of the Co adatom.

A rather interesting scenario can be observed in the cases of Co and Fe adatoms on a Re overlayer and of the Co adatom on Ir and Bi overlayers [see Figs. 4(b) and 4(c), respectively]. On the one hand, some peaks near the Fermi level have both electron and hole components, thus carrying the signature of a superconducting state. On the other hand, the electron down component is coupled to the hole down component, which is not possible in a spin-singlet type of superconducting state. This behavior can be identified only with the presence of some kind of a triplet pairing state.

C. Triplet order parameters

It is known that the fermionic nature of the electron implies that in the case of triplet pairing, the spatial component of the wave function has to be odd. In the context of a multiband Hamiltonian for bulk systems, this leads to even-parity, odd-orbital triplet states, which have been shown to be responsible for the experimentally observed simultaneous appearance of magnetism and the superconducting state in certain materials [39,40]. In these cases the translational invariance made it possible to introduce a proper parity operator for the whole system. Although translational invariance is broken for surfaces with an impurity, we can still expect spin-orbit coupling to induce triplet pairing if a singlet pairing state already exists, similar to the results in Refs. [40–42]. Such a state can be called an internally antisymmetric triplet (IAT). It is expected that the relativistic Andreev scattering process, captured accurately by the generalized multiple scattering theory for the superconducting state, will yield the largest contribution to the IAT, which is antisymmetric with respect to the orbital degrees of freedom. The formation of the IAT states can be easily understood within our formalism because during the solution of the relativistic Bogoliubov–de Gennes equations, spin-orbit-induced mixing occurs between the spin and orbital degrees of freedom together with the electron-hole character (see also Ref. [43]). In order to characterize this kind of pairing, one can define a DOS-like quantity, the energy-resolved IAT order parameter or IAT anomalous density, based on the norm of the energy-resolved elements of the off-diagonal Green’s function matrix. The way we calculate both the singlet and triplet (IAT) order parameters is described in detail

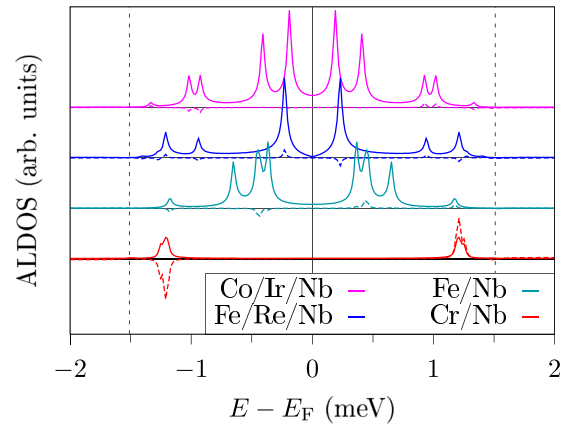


FIG. 5. Calculated anomalous local density of states (ALDOS) for some selected adatom systems. Dashed lines: singlet state order parameters; solid lines: IAT order parameters.

in the Appendix (see also Ref. [44]). In Fig. 5 the singlet and triplet state order parameters are plotted for selected adatom systems. When viewed together with the corresponding entries in Figs. 2 and 4, it is clear that both order parameters give visible peaks at those energies where YSR states occur. Among the presented cases, the singlet order parameter has sizable peaks only at the positions of the YSR states of the Cr/Nb(110) system. This is not surprising since the YSR state in this system was attributed to Cooper pair scattering, giving rise to both electron- and holelike components with opposite spin character. The IAT order parameter signals triplet YSR states in the case of Co/Bi/Nb(110) and Co/Ir/Nb(110) and for the Fe/Nb(110) case, where the singlet order parameter is negligible. Note that both order parameters are zero if there is no mixing between the electron- and holelike components. This verifies our classification of YSR states according to the kind of pairing state they represent: superconducting singlet, superconducting triplet, and normal state.

D. Magnetic orientation dependence of the YSR states

Let us now elaborate on another effect of the SOC in the calculations. Without SOC, the LDOS does not depend on the direction of the magnetic moment in either the normal or superconducting state. In the presence of SOC, the LDOS will significantly change versus the magnetic moment’s direction, so now we focus on how the energy of the YSR states changes if the magnetic moment is rotated. The direction of the magnetic moment of the adatom can be represented by azimuthal and polar angles, (ϑ, φ) , where the azimuthal angle ϑ is the angle with respect to the normal-to-surface direction (z), while the polar angle φ is the angle to the x axis if the moment is projected to the xy plane. As a representative example, let us consider the Co adatom on an Ir overlayer (see Fig. 6). On the baseline we plot the LDOS with $(\vartheta, \varphi) = (0^\circ, 0^\circ) (= z)$, and moving upwards, the curves follow each other in steps of 10° in the magnetic moment’s direction. First, we rotate the moment from the z axis to the x axis and then continue from x to y and, finally, back to z .

As shown in Fig. 4(c), in the ground state direction $z = (0^\circ, 0^\circ)$ of the Co/Ir/Nb(110) system there are five pairs

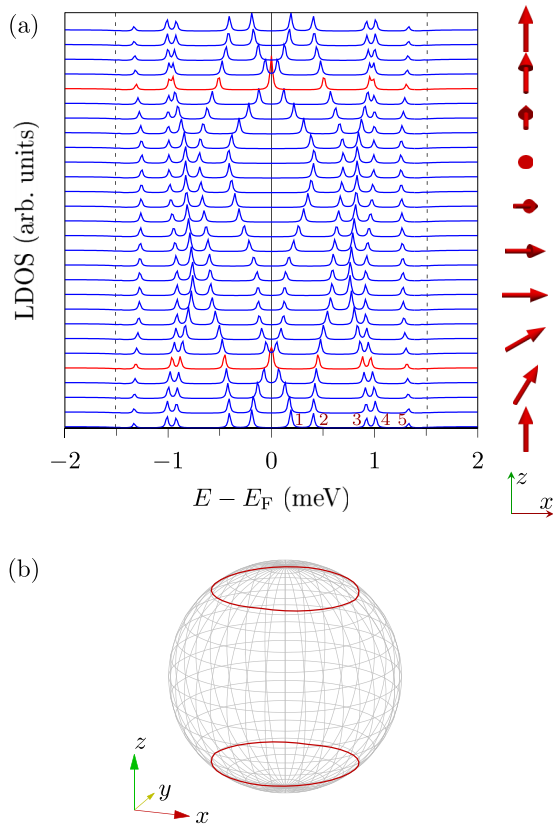


FIG. 6. (a) Calculated LDOS in the superconducting gap of a Co adatom on a Nb(110) surface covered by a single-atom-thick Ir overlayer as the magnetic moment of Co is rotated along a path between Cartesian axes, $z \rightarrow x$, $x \rightarrow y$, and $y \rightarrow z$. The direction of the magnetic moment for the corresponding LDOS is visualized by arrows on the right side. Between neighboring curves, there is a 10° difference in the direction of the magnetic moment, except the curves between $(50^\circ, 90^\circ)$ and $(30^\circ, 90^\circ)$, where the curve with a peak at zero energy, $(37^\circ, 90^\circ)$, is plotted instead. We used red for the curves containing a peak at zero energy. (b) Red lines denote the full paths on the unit sphere for which a zero bias peak can be found.

of peaks in the superconducting LDOS. In the following we label the YSR states by an integer: the YSR state nearest the Fermi energy is labeled 1, and the one nearest the edge of the gap is labeled 5. It is apparent from Fig. 6(a) that the position of the YSR state with the lowest energy (number 1) changes the most. Interestingly, this peak crosses the Fermi energy during the rotation of the magnetic moment, so at certain orientations of the magnetic moment, $(40^\circ, 0^\circ)$ and $(37^\circ, 90^\circ)$ [see Fig. 6(a)], there is a peak right at zero energy. This, of course, should not be mistaken for a topological phase, which may also have a peak at zero energy, just opposite; this points out that a peak at zero energy does not necessarily mean a topological state. It should be noted that peaks 4 and 5 seem to be rather insensitive to the orientation of the magnetic moment. In summary, we can conclude that the rotation of the magnetic moment influences the different YSR states in different ways, and there are more likely larger shifts in the position of the peak if it lies closer to the Fermi energy. It should be noted that a similar sensitivity of the YSR states was found theoretically for magnetic impurities on Pb(110) [43].

We have seen that in the case of the Co adatom on an Ir overlayer one of the YSR states crosses the Fermi energy twice. In Fig. 6(a) we consider a closed path in configuration space, for which an even number of Fermi level crossings is expected, excluding the special case when either of the extrema is at the Fermi energy, meaning that the peak turns back when reaching the Fermi energy, but then there is no Fermi level crossing at all. Because there are two orientations along the path with a zero-bias peak, we assume that Fermi level crossings can be found for a continuous set in the configuration space. Such configurations can be found, e.g., in two steps: first, change φ by a small angle, and then determine how to change ϑ so that the YSR state at zero energy is not shifted. Most naively, we can connect the two spin directions by a linear function, $\vartheta = 40^\circ - \varphi/30$ for $\varphi \in [0, 90^\circ]$. With calculations we confirmed that, indeed, there is a peak at zero energy for all orientations along this path, while the rest of the peaks (numbers 2–5) are slightly shifted. This path can easily be extended by taking into account the C_{2v} symmetry of the system, so that the magnetic configurations can be mirrored with respect to the xz and yz planes. The full path and its time-reversed pair (with opposite spin directions) are visualized in Fig. 6(b). We find that these paths are circles with a small oscillation in ϑ , so in this case the relative angle to the z axis, being the easy direction, is the key factor in regard to whether there is a peak at zero energy or not.

IV. CONCLUSIONS

Based on the band theoretical solution of the fully relativistic Bogoliubov–de Gennes equations, we performed a systematic study of the YSR states induced by magnetic impurities on a bare superconducting Nb(110) surface and a surface capped by a single atomic layer of Bi, Re, or Ir. Our most important finding is that the YSR states can be classified according to the pairing associated with them based on superconducting order parameters and that there are three kinds of YSR states: normal and singlet and triplet superconducting states. Although the appearance of the triplet states is exclusively linked to the presence of (strong) spin-orbit coupling, we demonstrated that spin-orbit coupling alone is not enough to predict which kind of a YSR state one may obtain in a given system. We also showed that there can be YSR states at zero energy along a continuous path in configuration space without any topological origin, which is also a direct consequence of the SOC. This fact may have important implications in more complicated systems in which non-Majorana zero-energy states or Majorana states may be observed. Our theoretical results highlight that one should be very cautious when interpreting zero-bias peaks observed in experiments.

ACKNOWLEDGMENTS

B.N., A.L., L.S., and B.U. acknowledge financial support from the National Research, Development, and Innovation Office (NRDI Office) of Hungary under Projects No. K131938 and No. K142652. B.N. and L.S. acknowledge support from the Ministry of Culture and Innovation and the NRDI Office within the Quantum Information National Laboratory of Hungary (Grant No. 2022-2.1.1-NL-2022-00004).

B.N. acknowledges the support from the ÚNKP-22-4-I New National Excellence Program of the Ministry of Culture and Innovation from the source of the NRDI Fund. The authors acknowledge KIFÜ for awarding us access to resources based in Hungary.

APPENDIX: DEFINITION OF THE SINGLET AND TRIPLET ORDER PARAMETERS

The calculations in this paper are based on the solution of the relativistic Kohn-Sham-Dirac Bogoliubov–de Gennes (KSDBdG) Hamiltonian:

$$H_{\text{DBdG}} = \begin{pmatrix} H_D(\vec{r}) & \Delta_{\text{eff}}(\vec{r}) \\ \Delta_{\text{eff}}^\dagger(\vec{r}) & -H_D^*(\vec{r}) \end{pmatrix}, \quad (\text{A1})$$

where $H_D(\vec{r}) = c\vec{\alpha}\vec{p} + (\beta - \mathbb{I}_4)c^2/2 + [V_{\text{eff}}(\vec{r}) - E_F]\mathbb{I}_4 + \beta\vec{\Sigma}\vec{B}_{\text{eff}}(\vec{r})$, where $\vec{\alpha} = \sigma_x \otimes \vec{\sigma}$, $\beta = \sigma_z \otimes \mathbb{I}_2$, $\vec{\Sigma} = \mathbb{I}_2 \otimes \vec{\sigma}$, $\vec{\sigma}$ denotes the Pauli matrices, \mathbb{I}_n stands for the identity matrix of order n , and $V_{\text{eff}}(\vec{r})$ and $\vec{B}_{\text{eff}}(\vec{r})$ are the effective potential and the exchange field, respectively. $\Delta_{\text{eff}}(\vec{r})$ is the effective 4×4 pairing potential matrix due to the four-component Dirac spinors. The KSDBdG equations are solved by assuming that the superconducting host (but only the host) has isotropic s -wave spin-singlet pairing as described in BCS theory. We evaluate the Green's function of the Hamiltonian (A1) according to Refs. [24,29] via multiple scattering theory. When integrating the Green's function in atomic cells n and m , the Green's function matrix $\{G_{QQ'}^{nm,ab}(z)\}$ can be defined, where z is the complex energy, a and b label the electron- and holelike components, and Q and Q' denote either relativistic angular momentum quantum numbers (κ, μ) , or orbital and spin quantum numbers $(\ell, m, s) = (L, s)$. Local quantities are obtained by considering site-diagonal elements of the Green's function matrix. The electron- or holelike local density of states is calculated according to

$$\text{LDOS}_n^a(\varepsilon) = -\frac{1}{\pi} \text{Im Tr}_Q \{G_{QQ'}^{nm,aa}(\varepsilon + i0)\}. \quad (\text{A2})$$

The appearance of the superconducting state is manifested in the local Green's function as nonzero elements in the electron-hole off-diagonal block. Hence, all the order parameters related to different pairing states should be derived from these elements. First, we define the following LDOS-like quantity to describe the energy resolution of the spin-singlet local order parameter:

$$\chi_S^n(\varepsilon) = -\frac{1}{\pi} \text{Im Tr}_L \mathcal{S}_s \{G_{LL',ss'}^{nm,eh}(\varepsilon + i0)\}, \quad (\text{A3})$$

where Tr_L denotes the trace in angular momentum space, while \mathcal{S}_s generates the spin singlet, $\mathcal{S}_s\{f(s, s')\} = \frac{1}{2}[f(\frac{1}{2}, -\frac{1}{2}) - f(-\frac{1}{2}, \frac{1}{2})]$. The energy-resolved local singlet order parameter shown in Fig. 5 has properties very similar to the electronic DOS and is often referred to as (energy-resolved) anomalous density.

We also define another DOS-like quantity to account for the energy-resolved IAT order parameter,

$$\bar{\chi}_{\text{IAT}}^n(\varepsilon) = \sum_{i=-1,0,1} \left\| -\frac{1}{\pi} \text{Im } \mathcal{A}_L \mathcal{T}_s^i \{G_{LL',ss'}^{nm,eh}(\varepsilon + i0)\} \right\|_F, \quad (\text{A4})$$

with the antisymmetrization in angular momentum space, $\mathcal{A}_L\{f_{LL'}\} = \{\frac{1}{2}(f_{LL} - f_{LL'})\}$, and the projections on spin triplets, $\mathcal{T}_s^0\{f_{ss'}\} = \frac{1}{2}(f_{\frac{1}{2},-\frac{1}{2}} + f_{-\frac{1}{2},\frac{1}{2}})$ and $\mathcal{T}_s^{\pm 1}\{f_{ss'}\} = f_{\pm\frac{1}{2},\pm\frac{1}{2}}$, while $\|M\|_F$ denotes the Frobenius norm of matrix M . The induced triplet superconductivity can be studied on an *ab initio* level by analyzing $\bar{\chi}_{\text{IAT}}(\varepsilon)$ [24,29].

As the YSR states are formed from atomic d orbitals, we may restrict the investigation of the triplet order parameter $\bar{\chi}_{\text{IAT}}$ at any given energy to those that couple only the $3d$ orbitals.

-
- [1] Yu Luh, *Acta Phys. Sin.* **21**, 75 (1965).
[2] H. Shiba, *Prog. Theor. Phys.* **40**, 435 (1968).
[3] A. I. Rusinov, *Zh. Eksp. Teor. Fiz. Pisma Red.* **9**, 146 (1968) [*JETP Lett.* **9**, 85 (1969)].
[4] S.-H. Ji, T. Zhang, Y.-S. Fu, X. Chen, X.-C. Ma, J. Li, W.-H. Duan, J.-F. Jia, and Q.-K. Xue, *Phys. Rev. Lett.* **100**, 226801 (2008).
[5] B. W. Heinrich, J. I. Pascual, and K. J. Franke, *Prog. Surf. Sci.* **93**, 1 (2018).
[6] S. Nadj-Perge, I. K. Drozdov, J. Li, H. Chen, S. Jeon, J. Seo, A. H. MacDonald, B. A. Bernevig, and A. Yazdani, *Science* **346**, 602 (2014).
[7] Y. Kim, M. Cheng, B. Bauer, R. M. Lutchyn, and S. Das Sarma, *Phys. Rev. B* **90**, 060401(R) (2014).
[8] M. Ruby, F. Pientka, Y. Peng, F. von Oppen, B. W. Heinrich, and K. J. Franke, *Phys. Rev. Lett.* **115**, 197204 (2015).
[9] Y. Peng, F. Pientka, L. I. Glazman, and F. von Oppen, *Phys. Rev. Lett.* **114**, 106801 (2015).
[10] R. Pawlak, M. Kisiel, J. Klinovaja, T. Meier, S. Kawai, T. Glatzel, D. Loss, and E. Meyer, *npj Quantum Inf.* **2**, 16035 (2016).
[11] M. Ruby, B. W. Heinrich, Y. Peng, F. von Oppen, and K. J. Franke, *Nano Lett.* **17**, 4473 (2017).
[12] L. Schneider, P. Beck, T. Posske, D. Crawford, E. Mascot, S. Rachel, R. Wiesendanger, and J. Wiebe, *Nat. Phys.* **17**, 943 (2021).
[13] C. Mier, J. Hwang, J. Kim, Y. Bae, F. Nabeshima, Y. Imai, A. Maeda, N. Lorente, A. Heinrich, and D.-J. Choi, *Phys. Rev. B* **104**, 045406 (2021).
[14] L. Schneider, P. Beck, J. Neuhaus-Steinmetz, L. Rózsa, T. Posske, J. Wiebe, and R. Wiesendanger, *Nat. Nanotechnol.* **17**, 384 (2022).
[15] E. Liebhaber, L. M. Rütten, G. Reecht, J. F. Steiner, S. Rohlf, K. Rossnagel, F. von Oppen, and K. J. Franke, *Nat. Commun.* **13**, 2160 (2022).
[16] K. J. Franke, G. Schulze, and J. I. Pascual, *Science* **332**, 940 (2011).

- [17] N. Hatter, B. W. Heinrich, M. Ruby, J. I. Pascual, and K. J. Franke, *Nat. Commun.* **6**, 8988 (2015).
- [18] N. Hatter, B. W. Heinrich, D. Rolf, and K. J. Franke, *Nat. Commun.* **8**, 2016 (2017).
- [19] L. Farinacci, G. Ahmadi, M. Ruby, G. Reecht, B. W. Heinrich, C. Czekelius, F. von Oppen, and K. J. Franke, *Phys. Rev. Lett.* **125**, 256805 (2020).
- [20] P. Beck, L. Schneider, L. Rózsa, K. Palotás, A. Lászlóffy, L. Szunyogh, J. Wiebe, and R. Wiesendanger, *Nat. Commun.* **12**, 2040 (2021).
- [21] S. Kezilebieke, M. Dvorak, T. Ojanen, and P. Liljeroth, *Nano Lett.* **18**, 2311 (2018).
- [22] J. Brand, S. Gozdzik, N. Néel, J. L. Lado, J. Fernández-Rossier, and J. Kröger, *Phys. Rev. B* **97**, 195429 (2018).
- [23] S. Kezilebieke, R. Žitko, M. Dvorak, T. Ojanen, and P. Liljeroth, *Nano Lett.* **19**, 4614 (2019).
- [24] B. Nyári, A. Lászlóffy, L. Szunyogh, G. Csire, K. Park, and B. Ujfalussy, *Phys. Rev. B* **104**, 235426 (2021).
- [25] T. G. Saunderson, J. F. Annett, G. Csire, and M. Gradhand, *Phys. Rev. B* **105**, 014424 (2022).
- [26] P. Beck, B. Nyári, L. Schneider, L. Rózsa, A. Lászlóffy, K. Palotás, L. Szunyogh, B. Ujfalussy, J. Wiebe, and R. Wiesendanger, *Commun. Phys.* **6**, 83 (2023).
- [27] P. Beck, L. Schneider, L. Bachmann, J. Wiebe, and R. Wiesendanger, *Phys. Rev. Mater.* **6**, 024801 (2022).
- [28] B. Lazarovits, L. Szunyogh, and P. Weinberger, *Phys. Rev. B* **65**, 104441 (2002).
- [29] G. Csire, A. Deák, B. Nyári, H. Ebert, J. F. Annett, and B. Ujfalussy, *Phys. Rev. B* **97**, 024514 (2018).
- [30] L. Szunyogh, L. Udvardi, J. Jackson, U. Nowak, and R. Chantrell, *Phys. Rev. B* **83**, 024401 (2011).
- [31] A. Lászlóffy, L. Udvardi, and L. Szunyogh, *Phys. Rev. B* **95**, 184406 (2017).
- [32] A. Lászlóffy, K. Palotás, L. Rózsa, and L. Szunyogh, *Nanomaterials* **11**, 1933 (2021).
- [33] M.-H. Wu, E. Thill, J. Crosbie, T. G. Saunderson, and M. Gradhand, *Phys. Rev. B* **107**, 094409 (2023).
- [34] D.-J. Choi, C. Rubio-Verdú, J. de Bruijckere, M. M. Ugeda, N. Lorente, and J. I. Pascual, *Nat. Commun.* **8**, 15175 (2017).
- [35] H. Ebert, H. Freyer, A. Vernes, and G.-Y. Guo, *Phys. Rev. B* **53**, 7721 (1996).
- [36] See Supplemental Material at <http://link.aps.org/supplemental/10.1103/PhysRevB.107.224515> for calculations in which the spin-orbit coupling was scaled to zero.
- [37] G. Csire, J. Cserti, and B. Újfalussy, *J. Phys.: Condens. Matter* **28**, 495701 (2016).
- [38] H. Kim, A. Palacio-Morales, T. Posske, L. Rózsa, K. Palotás, L. Szunyogh, M. Thorwart, and R. Wiesendanger, *Sci. Adv.* **4**, eaar5251 (2018).
- [39] S. K. Ghosh, G. Csire, P. Whittlesea, J. F. Annett, M. Gradhand, B. Újfalussy, and J. Quintanilla, *Phys. Rev. B* **101**, 100506(R) (2020).
- [40] G. Csire, J. F. Annett, J. Quintanilla, and B. Újfalussy, *Phys. Rev. B* **106**, L020501 (2022).
- [41] S. K. Ghosh, M. Smidman, T. Shang, J. F. Annett, A. D. Hillier, J. Quintanilla, and H. Yuan, *J. Phys.: Condens. Matter* **33**, 033001 (2021).
- [42] G. Csire, B. Újfalussy, and J. F. Annett, *Eur. Phys. J. B* **91**, 217 (2018).
- [43] K. Park, B. Nyári, A. Lászlóffy, L. Szunyogh, and B. Ujfalussy, *New J. Phys.* **25**, 033022 (2023).
- [44] B. Nyári, A. Lászlóffy, G. Csire, L. Szunyogh, and B. Újfalussy, *Research Square*.